Mine Water and the Environment (2023) 42:618–638
https://doi.org/10.1007/s10230-023-00960-4

TECHNICAL ARTICLE

Remote Sensing Data and Indices to Support Water Management: A Holistic Post-mining Approach for Lignite Mining in Greece

Georgios Louloudis[1] · Christos Roumpos[1] · Eleni Mertiri[1] · Francis Pavloudakis[2] · Konstantinos Karalidis[1]

Received: 13 February 2023 / Accepted: 2 November 2023 / Published online: 8 December 2023

Abstract

Entering the coal phase-out era, major priorities of the Greek lignite mining industry are sustainable mine closure, land reclamation, and planning for long-term and sustainable land repurposing scenarios. A holistic and digitally enabled approach to water management could lead to effective strategic planning in the coal phase-out era. This research proposes an integrated approach to evaluate the hydrological profile of a large and complex open pit lignite mining area based on remote sensing data. This framework included processing of satellite images in different bands and an evaluated digital elevation model of an ≈170 km^2 area within the Ptolemais Basin, northern Greece, that has extensive surface lignite mining. Several spectral (*SMI, RIP, NDVI, NDWI, MNDWI*) and topographic (*SPI, TWI, LS*) indices were investigated, providing details of spatial and temporal variations in the terrestrial water cycle. The analysis permitted the hydrological characteristics of the study area to be mapped with sufficient accuracy. Water bodies, low-flowing streams, water flow direction, vegetation cover, erodible areas, locations with water accumulation, and areas with high soil moisture were identified. A major additional outcome of this research was the construction of flood-susceptibility maps introducing several hydrological parameters in a fuzzy model. The results indicated several areas inside the mining area with high flood susceptibility. These results were subsequently validated through PPC flood event reports during heavy rainfalls and events reported in the National River Basin Management plans. Using high-resolution digital elevation models and remote sensing data processing to identify hazards, like flooding, could improve land use planning and water management strategies.

Keywords Ptolemais Basin · Fuzzy model · Flood hazard susceptibility · Satellite imaginary · Land use planning

Introduction

Remote sensing is increasingly appreciated, especially in poorly gauged areas where no monitoring network exists or in-situ monitoring provides only sparse hydrological data (Lakshmi 2015; Mendiguren et al. 2017). Also, remote sensing technologies have been used in developing large-scale hydrological models (Wanders et al. 2014; Xu et al. 2014; Yan et al. 2022). Much literature has been published on remote sensing, investigating indices that can help us understand and subsequently evaluate the spatial and temporal variations in the terrestrial water cycle. Methods have been developed to process satellite images to map topographic features and monitor land cover via calculated indices. Soil moisture index (*SMI*) is one of the most widely used indices that is key to calculating daily soil moisture content and forecasting trends. *SMI* can provide an accurate discharge simulation (Gomis-Cebolla et al. 2022; Wanders et al. 2014) and is related to agricultural drought (Berg and

✉ Christos Roumpos
c.roumpos@dei.gr

Georgios Louloudis
g.louloudis@dei.gr

Eleni Mertiri
e.mertiri@dei.gr

Francis Pavloudakis
fpavloudakis@uowm.gr

Konstantinos Karalidis
kkaralidis13@gmail.com

[1] Dept. of Mining Engineering and Closure Planning, Public Power Corporation of Greece, Athens, Greece

[2] Dept. of Mineral Resources Engineering, University of Western Macedonia, Kozani, Greece

Sheffield 2018; Sohrabi et al. 2015). The normalized difference vegetation index (*NDVI*), normalized difference water index (*NDWI*), and modified normalized difference water index (*MNDWI*) (Xu 2006) also have great value in calculating vegetation cover, leaf water, and the presence of water bodies, making them useful for evaluating vegetation health and drought conditions (Acharya et al. 2016; Caturegli et al. 2020; Gomis-Cebolla et al. 2022; Rad et al. 2021). *MNDWI* can accurately extract water bodies and provide information on the presence of surface water, as it enhances the contrast between water features and areas with built-up land, soil, and vegetation.

Other studies have reported topographical indices that can be deduced by processing digital elevation model (DEM) data. For example, the topographic wetness index (*TWI*) is the most well-known and widely used method to measure the relative soil moisture status of a catchment area and evaluate pollution risk (Beven and Kirkby 1979; Buchanan et al. 2014; Moore et al. 1991). Stream power index (*SPI*) is also widely used to estimate the probability of erosion due to flowing water and evaluate surface runoff at the upstream drainage area (Byrne 2018; Danielson 2013; Ghunowa et al. 2021; Jacoby et al. 2011; Moore et al. 1991). Another important index is the slope length (*LS*) factor (Moore and Burch 1986; Moore and Wilson 1992), which describes drainage density and is used to predict erosion.

Concerning the dynamic process of environmental changes, the study of land use change has grown in importance, sparking important research globally (Zhao et al. 2022). Topography can influence land use and land cover (LULC), affecting the regional structure. Additionally, the landscape and LULC can alter the water balance, as the groundwater recharge and surface runoff are affected. Therefore, in the case of surface mining, where landscape and LULC can change drastically during the development of mines and after exploitation ends, the examination and selection of proper future land uses depend on elevation and slope (Yu et al. 2010) and their dynamic relationship with the proposed land use spatial patterns. These areas frequently encounter rapid and meaningful shifts in LULC as a result of mining operations (Sonter et al. 2014). Therefore, policies concerning the management and protection of waters is included in the license to operate and should receive attention in the post-mining phase to limit social and environmental impacts.

The lignite mining sector of Greece, represented mainly by the Public Power Corporation (PPC) of Greece, is facing a transition stage, to decommission coal operations and adopt environmentally-friendly technologies (Pavloudakis et al. 2020). Transitioning to a policy of zero discharge of "uncontrolled" mine water is a great economic and ecological challenge. Adopting Green policies is considered a high priority for the PPC, which has recently designed core strategies in the renewable energy sources (RES) sector. As a result, multi-level planning is critical within the framework of the environmental policy. The need for compliance with national and international laws targeting the design and implementation of practical and sustainable solutions while considering a circular economy, climate change, and biodiversity is an added challenge. Planning should set specific barriers for environmental and socioeconomic character and should include the development of sustainable land uses and effective policies for the optimal use of the area, aiming to support continuous environmental improvement.

Approaching the problem holistically is of great importance, as mines in Greece must comply with strict legislation that makes proper and efficient management of water resources mandatory. Furthermore, implementation of the Water Framework Directive and Floods Directive (European Commission, Directorate-General for Environment 2021) is obligatory for sustainable ground and surface water management. The mines have to consider many aspects of water management and identify all actions and measures to be taken within the river basin district to deliver the objectives of the Water Framework and Floods Directives, including their "daughters", as described in National River Basin Management Plans (Government Gazette 4676/B/29.12.2017 2017, 2689/B/6.07.2018 2018).

Mining areas have complex terrains and the effects of any LULC change are likely to exhibit considerable spatial heterogeneity that depend on topography-related variables (Zhang et al. 2021). In open pit mining-influenced areas, the topography changes during exploration, excavation, and operational phases. Therefore, a topographic study is essential to smooth the transition from lignite to RES sites and other new land uses. In a system with complex hydrogeological flow systems, topographic and remote sensing studies can provide a helpful information for effective mine water management, especially when considered temporally at large scales (Sonter et al. 2014). Such information may include spatial and temporal distribution of soil moisture, soil degradation, vegetation cover, surface runoff, lateral movement of rainwater along the hillslope, and its accumulation in certain places, and water quality classification of pit lakes (Pu et al. 2019).

The objective of this study was to investigate the value of geographic information systems (GIS) using high-quality remote sensing data and novel spectral indices to analyse the hydrological characteristics for the Ptolemais Basin in northern Greece. Thus, satellite images in different bands and topographic indices were analysed to provide a holistic post-mining approach for lignite mining. The complexity of the hydrologic flow patterns in this area presents challenges to land use repurposing and post-mining reclamation strategies. We also evaluated various options regarding economic transitions, providing a tool to highlight areas with

potentially high flood susceptibility in the surrounding area and offer efficient land use reclamation insights. Combining topographic and spectral indices can provide a more holistic perspective to support water management in complex post-mining areas as it considers not only the spectral characteristics of the terrain but also its physical features. This approach could aid future risk and water management assessments by identifying hazards associated with flooding.

Research Area—Geomorphological and Hydrogeological Setting

The research area is located in the Ptolemais lignite-bearing basin in northern Greece, where the PPC currently operates three open cast lignite mines: Mavropigi, Kardia, and South Field (Fig. 1)(Roumpos et al. 2018). During operation, inside and outside dumping was conducted, mainly with spreaders (continuous surface mining) and occasionally with trucks and loaders (non-continuous surface mining). The mining activities in the south Ptolemais lignite-bearing area extend ≈ 14.5 km towards the northwest and southeast. In 2022, the dumping area covered ≈ 82 km^2 (≈ 75% of the total area), while excavation activities included an additional 28 km^2 (≈ 25% of the total area). It is worth mentioning that the area of mining activities (Fig. 2) considers the expansion of the lignite mines until final closure in 2028.

The mines are surrounded by the Vermion, Askion, and Skopos mountains (Fig. 1), within a complex meandering stream network. Rainwater flows into the Soulou River and discharges into Vegoritis Lake, the final receiving body of the surface runoff of the closed hydrological Ptolemais Basin (Dimitrakopoulos and Grigorakou 2004; Louloudis 1991) north of the research area. The Soulou River constitutes the primary water discharge, which makes monitoring and evaluating water quality a priority to protect the natural lake.

The geology of the Ptolemais Basin is dominated by Tertiary and Late Miocene to Pleistocene sediments (Fig. 2). Based on their petrophysics, the Tertiary strata consists mainly of intercalations of high permeability (sands, conglomerates) and low permeability layers (clays, silts, fluvial deposits, marls, lignites) overlying a Paleozoic basement consisting of schists, ophiolites, and granites followed by Mesozoic limestones, volcanic and flysch overburden sediments (Koukouzas et al. 2010; Pavloudakis et al. 2020). The Tertiary lignite-bearing sequence consists of intercalations of marls and lignites, and has an average thickness ranging from 80 to 140 m (Roumpos et al. 2015). Hydrologically, this sequence separates the upper unconfined Sarigiol

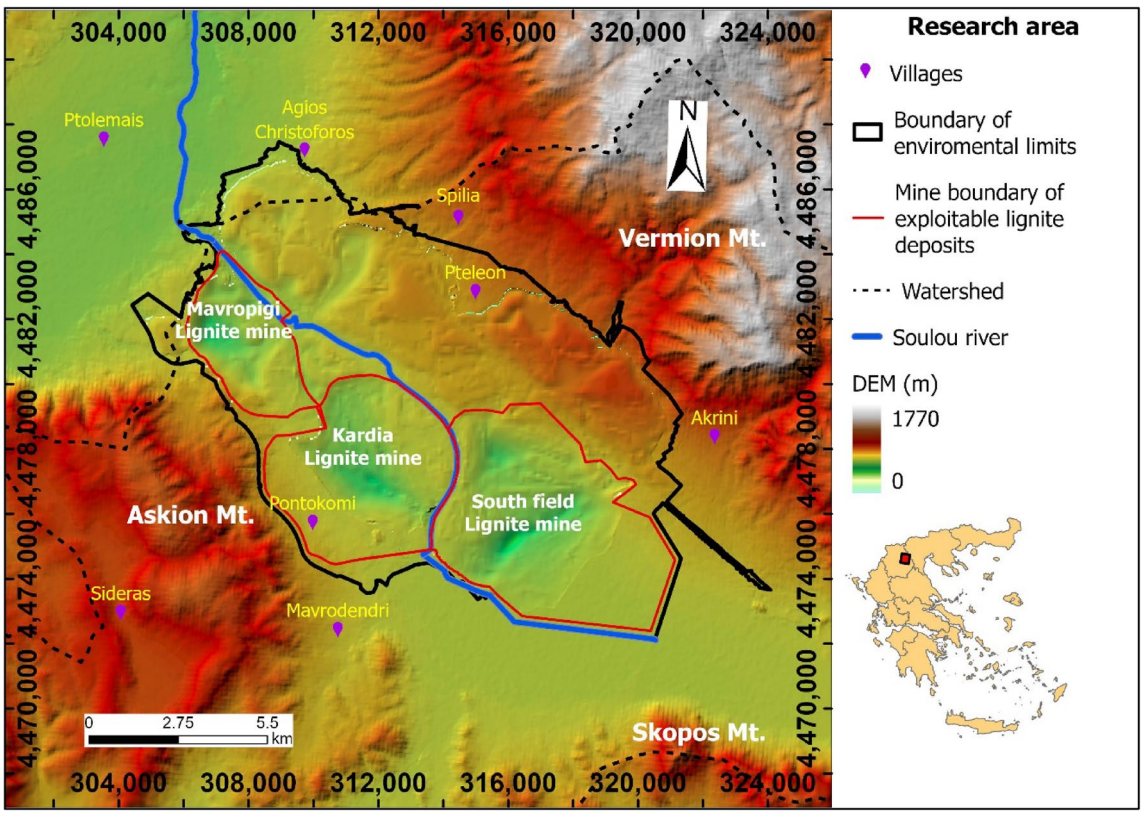

Fig. 1 Research area and location of the Ptolemais lignite mines, northern Greece

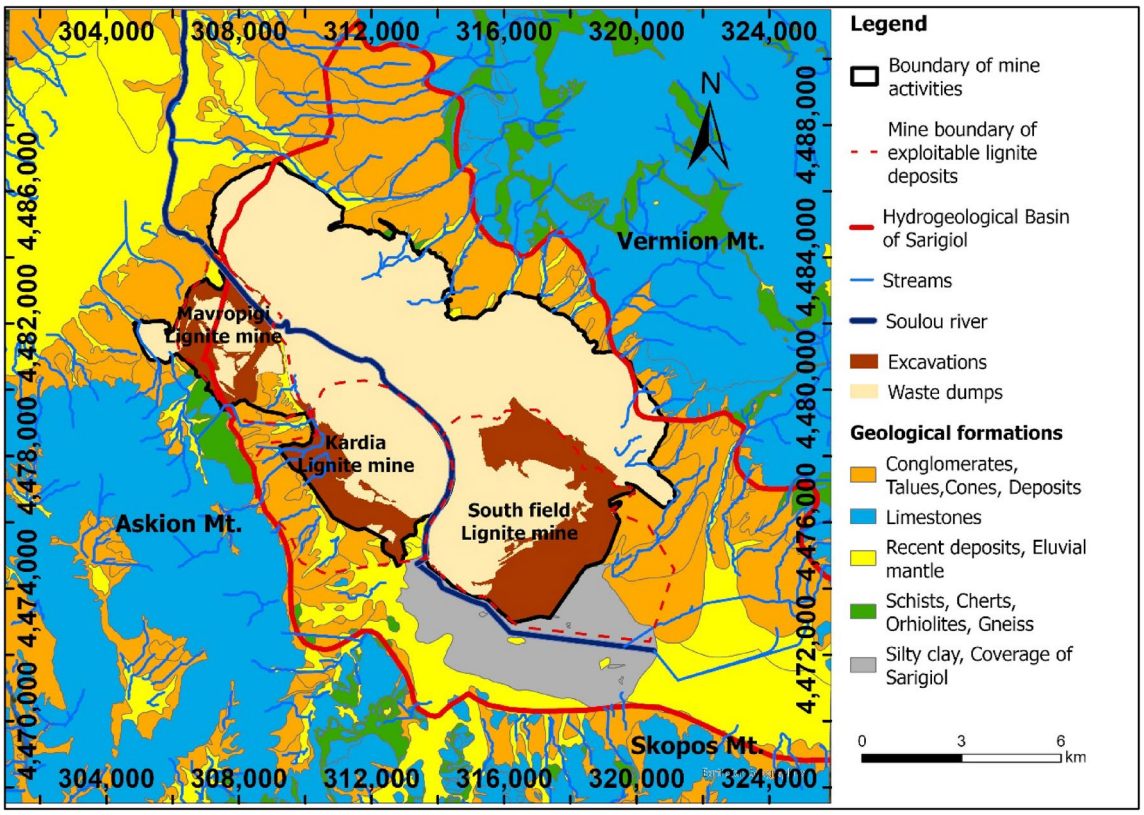

Fig. 2 Simplified geological map of the Ptolemais Basin, northern Greece. The mining area with the waste dumps and excavations is masked out (no geological formations are evident inside the boundary of mine activities

aquifer in the Quaternary sediments from the lower Komanos aquifer and is superimposed by an impermeable lignite sequence and marl and clayey formations. The Sarigiol aquifer behaves as a distinct aquifer consisting of a hydraulically connected network of superposed water-bearing horizons (Louloudis 1991; Louloudis et al. 2022). The network is developed inside the loose, unconsolidated Tertiary and Quaternary formations and is not connected in its whole extent with the karst water of the basin's mountainous surroundings. Its thickness ranges from 20 to 90 m (Modis et al. 2022; Roumpos et al. 2015) and exhibits hydraulic conductivities on the order of $K_f = 1.71 \times 10^{-4}$ to 2.00×10^{-6} m/s (Louloudis 1991).

Due to the nature of the mining activities (i.e. open pit), the general overflow is towards the surface lignite mines and into the Soulou River, while part of the surface runoff infiltrates and recharges local aquifers, i.e. the Sarigiol aquifer. Figure 3 provides a representative hydrogeological cross-section of the open pits, highlighting the main hydrogeological units in the research area.

The land uses in the Ptolemais area are depicted in the Fig. 4. Inside the boundary of mine activities, the artificial surfaces refer to the waste dumps and excavations while outside the boundary of mine activities, the artificial surfaces are paved roads, industrial areas, power plants, and livestock farms. In addition, the LULC map clearly illustrates that the mining activity areas are surrounded by large expanses of agricultural land, while the typical land cover on the Vermion, Askion, and Skopos mountains is forest. Besides the human-influenced surfaces within the mining boundary, the predominant LULC of the area are agriculture and forest.

Based on in-site measurements made by Papakōnstantinu (1979), the Vermion streams' discharge in the Ptolemais Basin is an insignificant contributor to surface runoff. Regarding the water balance in the Sarigiol sub-basin on a timescale of a 15-year hydrological cycle (2006–2021) (Louloudis et al. 2022), only 15% of the total annual precipitation percolates and recharges the Sarigiol aquifer, while evapotranspiration is on the order of ≈ 73% and the surface runoff is ≈ 12%. Depending on the groundwater level, either the Soulou River recharges the Sarigiol aquifer or the aquifer seeps into the river. During mining and to ensure safety on-site, groundwater is pumped from the dewatering wells around the perimeter of the mines and water is pumped from sumps located inside the open pits. It is calculated that in the year 2021, ≈ 95% of the total pumped water was discharged into the Soulou River. However, intensive irrigation during the dry season (May to October), consumes part of

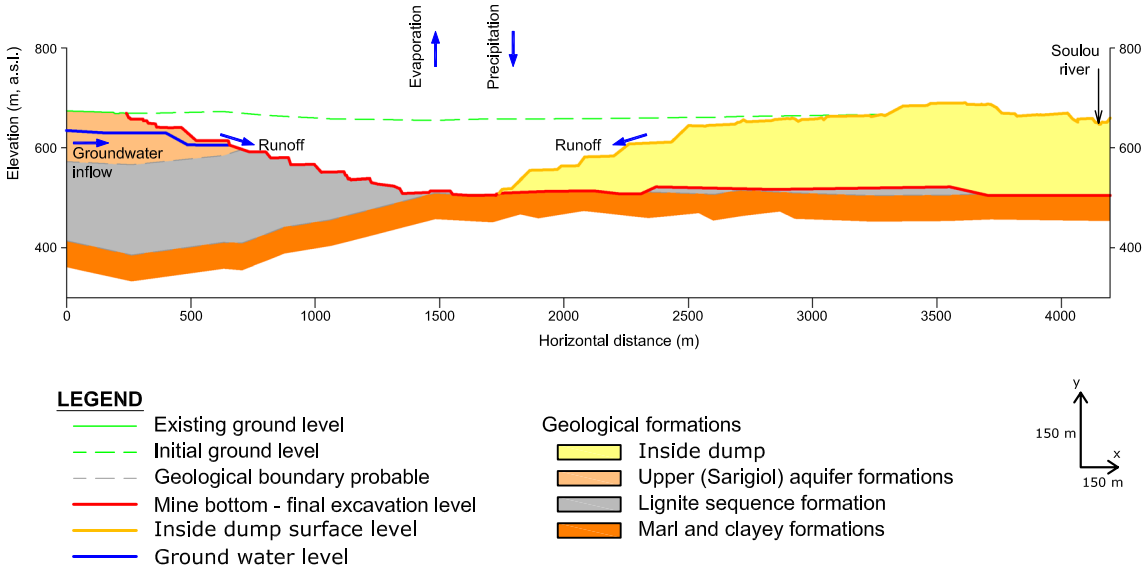

Fig. 3 Representative hydrogeological cross-section of the open pits, Ptolemais Basin, northern Greece. The upper aquifer (Sarigiol) is formed over lignite sequence, whereas the lower aquifer (Komanos) is formed below the impermeable marl and clayey formations

the discharged water via pumping from the river. Based on in-situ measurements of the Soulou River discharge at the northern boundary of the Mavropigi mine during the year 2021, ≈ 66 Mm^3 of water was directed into Vegoritis Lake situated to the north of the basin, of which 30 Mm^3 of water (≈ 45%) was PPC mine- and processed-water.

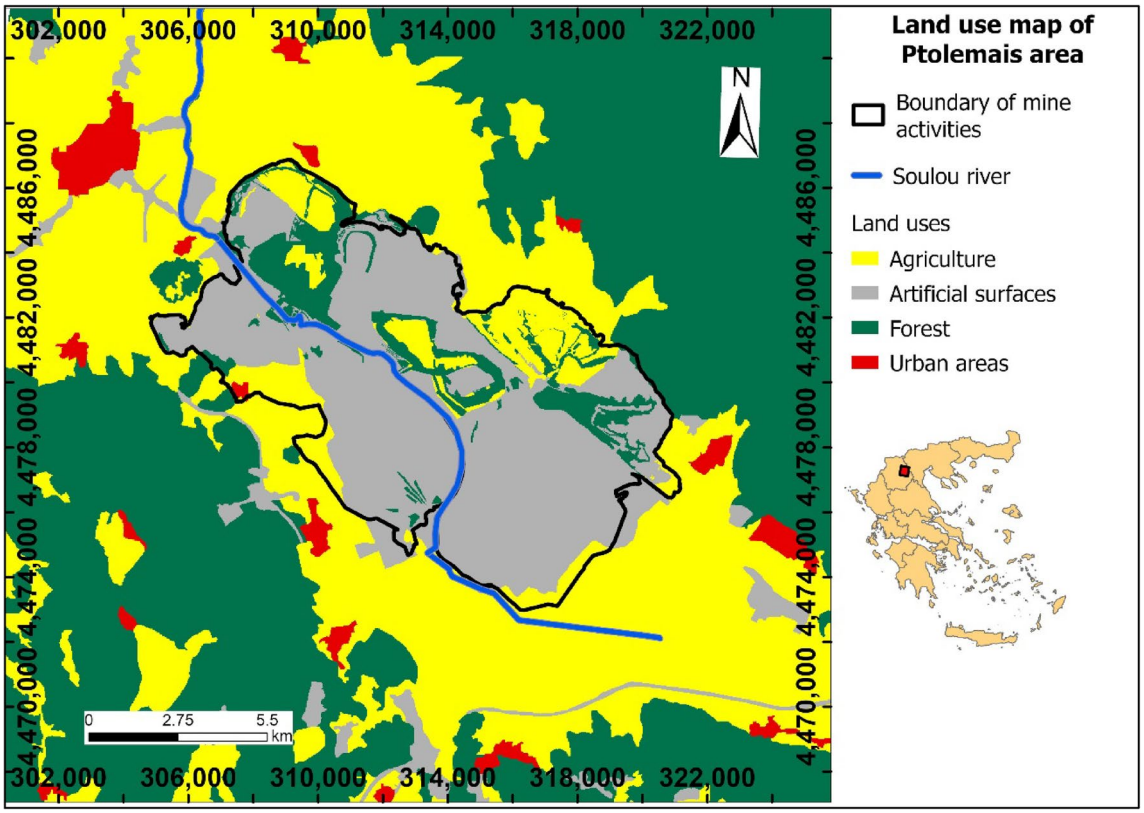

Fig. 4 Land uses in the Ptolemais Basin, northern Greece

The net monthly discharge of the Soulou River without the contributions from PPC is presented in Fig. 5A for years 2018–2021. In this figure, the Soulou discharge is correlated with the precipitation obtained from Kozani WMO no. 16 632 weather station (recorded by the Hellenic National Meteorological Service). The net discharge (Fig. 5A) represents the difference between the discharge of the Soulou River, measured north of the mining area at the exit of Sarigiol basin (north of the Mavropigi lignite mine) and the mine- and processed-waters of the PPC power plants discharged into the Soulou River, south of the mining area (the South Field lignite mine). The net discharge becomes negative when the rejected quantities of the mine and the processed water of power plants are higher than the quantities that finally end up at the exit of the basin. Negative net values are evident in summer months, which correlates to the irrigation period when water is pumped from Soulou River and thus, less end up at the Basin exit. Additionally, due to low precipitation during the summer (dry season), runoff discharge is very low and thus, the negative values are also derived due to evaporation processes in the Soulou River.

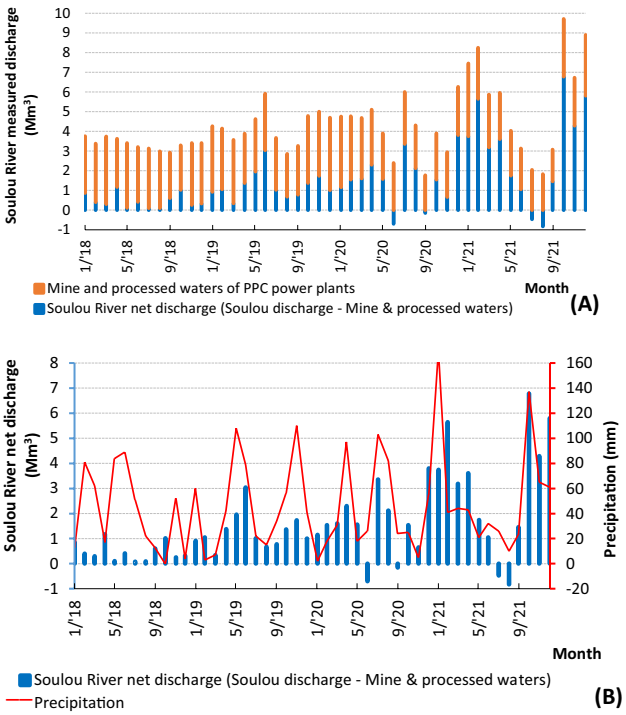

Fig. 5 Monthly discharge of the Soulou River for the period 2018–2021: **A** net discharge of the river and mine and processed waters of PPC power plants, and **B** net discharge of the river correlated with the monthly precipitation obtained from Kozani WMO No16 632 weather station (recorded by the Hellenic National Meteorological Service). Since runoff discharge is very low due to low precipitation in dry seasons, the negative values derived correspond to evaporation processes in Soulou river and also, the irrigation during summer months (during summer months water is occasionally pumped from Soulou River and is used for irrigation)

Material and Methods

High-resolution satellite images in different bands and DEMs were acquired and processed in this study (Table 1). Two distinct representative dates were chosen to depict the hydrological profile of the area of interest during two separate seasons (winter and summer). The satellite images selected were not taken during extreme weather events (i.e. large storms or other atmospheric phenomena that could skew the data captured in the images used). This approach was used to encompass the diverse hydrological characteristics exhibited during distinct seasons. Specifically, the summer date was selected to capture conditions marked by intensive irrigation and prolonged drought periods, while the winter date was chosen to represent circumstances characterized by abundant rainfall and the absence of irrigation.

Table 1 Data sources

Data	Type (spatial resolution in meters)	Source	Date
Sentinel-2 MSI LEVEL 2A	Raster grid (20 × 20 m)	ESA Copernicus https://scihub.copernicus.eu	24-12-2021
Landsat 8 OLI/ TIRS C2 L2	Raster grid (30 × 30 m)	USGShttps://earthexplorer.usgs.gov/	26-07-2022
Precipitation (mm)	Data table	National Observatory of Athens (NOA) https://www.meteo.gr/Gmap.cfm	01-01-2021 until 31-12-2021
DEM	Raster grid (25 × 25 m)	Copernicus (EU-DEM) for the area outside the boundary of the mines' environmental limits https://land.copernicus.eu/	01-11-2022
DEM	Raster grid (2 × 2 m)	PPC topographical data for the area within the boundary of the mines' environmental limits	16-06-2022
Map (topographical data)	Data image (scale 1:50,000)	Hellenic Military Geographical Service https://www.gys.gr/hmgs-archivedmaps.html	1970

Furthermore, the selected images were extracted with less than 5% cloud cover to provide good areal coverage. In addition, it is important to note that the analysis results are limited to the range of pixel sizes available, as access to higher resolution images is often restricted or not freely accessible. Higher resolution can lead to more accurate and finer details results by capturing smaller features and providing a more realistic representation of the produced maps. On the other hand, lower resolution can smooth out important characteristics while capturing the important geographical and topographical features. For that reason, accessing higher resolution images could alter the results of this study by providing more accurate and localized information. However, whether resolution is a major bottleneck depends on the specific goals and available resources. In this research, the spatial resolution is considered acceptable, given the size of the study area and the available data sources.

The topography largely controls the spatial variation of hydrological conditions, such as soil moisture, groundwater flow, and slope stability. Topography and elevation can also influence precipitation patterns, with respect to the quantity and type (i.e., snow, rain). Therefore, topographic indices (summarized in Table 2) were used to describe the spatial soil moisture patterns and identify erosion processes and potential in the streams of the wider area. These indices are also considered reliable predictors of locations of ephemeral gullies (Jacoby et al. 2011; Moore et al. 1991), which are related to erosion processes associated with heavy rainfall events. However, the threshold values (Moore and Burch 1986) of the derived indices may differ depending on the area because of the different soil properties. These topographic indices were calculated directly from the DEMs for the entire Ptolemais Basin area.

The stream power index (*SPI*) is a compound topographic attribute. It is a measure of the erosive power of flowing water based on the assumption that the discharge is proportional to a specific catchment area (Byrne 2018; Danielson 2013; Ghunowa et al. 2021; Moore et al. 1991). It generally predicts the probability of net erosion in areas of profile and tangential convexity (flow acceleration and convergence zones) and net deposition in areas of profile concavity (zones of decreasing flow velocity).

Table 2 Hydrological topography indices

Topography indices	Equation [1]	References
Power Stream Index	$SPI = As \bullet tanb$	Moore et al. (1991)
Topographic Wetness Index	$TWI = \ln(a/tanb)$	Beven and Kirkby (1979), Moore et al. (1991)
Slope length and steepness factor	$LS = (As/22.13)^{0.6}(sinb/0.0896)^{1.3}$	Moore and Burch (1986), Moore and Wilson (1992)

[1]where *As* is the catchment's area, *b* is the local slope gradient measured in degrees, an *a* is the total cumulative upslope area drained through a point per unit contour length

Beven and Kirby (1979) first established the topographic wetness index (*TWI*), which is considered one of the most useful compound terrain derivatives in hydrology and ecology (Buchanan et al. 2014). This index combines the water supply from the upslope catchment region and the downslope water drainage for each cell in a DEM (Kopecký et al. 2021). Therefore, the *TWI* was developed to estimate relative surface wetness and, consequently, hydrologic responsiveness throughout a watershed (Meles et al. 2020).

The slope length and steepness factor (*LS*) calculates the soil erosion based on the slope length (*L*) and steepness factor (*S*), which are computed based on the DEM. This index determines the effect of topography in a specific area and how intense the erosion is.

Except for the DEM processing, satellite image processing methods were also applied (Table 3). The acquired satellite imagery has undergone atmospheric correction in advance, a process carried out based the antecedent Level-1C products from which they were derived. Moreover, these satellites have undergone corrections to mitigate the

Table 3 Hydrological spectral indices

Topography indices	Equation [1]	Reference
Normalized Difference Vegetation Index	$NDVI = (NIR - RED)/(NIR + RED)$	Rouse et al. (1974)
Normalized Difference Water Index	$NDWI = (GREEN - NIR)/(GREEN + NIR)$	McFeeters (1996)
Modified Normalized Difference Water Index	$MNDWI = (GREEN - MIR)/(GREEN + MIR)$	Xu (2006)
Rainfall Infiltration Potential	$RIP = R_{av} * I_c$	Voudouris et al. 2007)
Soil Moisture Index	$SMI = (LST_{MAX} - LST)/(LST_{MAX} - LST_{MIN})$	Saha et al. (2018)

[1]where *NIR* equals the Top of Atmosphere (TOA)reflectance value of the near-infrared band (nm), *RED* defines the TOA reflectance value of the red band (nm), *GREEN* describes the TOA reflectance value of the green band (nm), *MIR* represents a middle (shortwave) infrared band, R_{av} is the average annual rainfall, I_c is the infiltration coefficient, *LST* is the temperature value for a given *NDVI* while the LST_{MAX} and LST_{MIN} are the maximum and minimum land surface temperatures for a given*NDVI*

influence of air molecule scattering, as well as the absorbing and scattering impacts of atmospheric gases (Copernicus 2023). Furthermore, Sentinel-2 satellite imagery was used to calculate *NDWI* and M*NDWI*, while Landsat-8 was used for the other indices. The thermal band of Landsat-8 was taken to calculate the *SMI* index. To calculate the *NDWI* and *MNDWI*, the bands 3 (central wavelength 560 nm) and 8 (central wavelength 842 nm) were used as well as the bands 3 and 11 (central wavelength 1610 nm), respectively. Moreover, the bands 4 (0.630 to 0.680 μm) and 5 (0.845 to 0.885 μm) were used to calculate the *NDVI*.

These methods can be useful for monitoring and quantifying spatial and temporal geophysical variables, such as water features and land cover over different landscapes on a temporal and regional scale (Tang et al. 2020). Thus, the combination of the aforementioned spectral bands, characterized by their high spatial resolution, can yield outcomes of heightened precision in relation to hydrological information.

The *NDVI* was established to estimate and evaluate vegetative coverage (Louloudis and Stathopoulos 2019), while the *NDWI* combined with the *MNDWI* were established to maximize the reflectance of water to identify water bodies, and thus estimate the vegetation water content in different crops (Acharya et al. 2016; Liang et al. 2020). In addition, the soil moisture index (*SMI*) was generated to identify the moisture of the soil during the summer months. The rainfall infiltration potential (*RIP*) was calculated (Voudouris et al. 2007) to determine the infiltration potential of the annual precipitation based on the geological formation. The *RIP* was calculated as a product of the infiltration coefficient and annual rainfall (Stathopoulos 2019). Based on the geological formations encountered in the area, infiltration coefficients were adopted from similar geological formations in Greece (Voudouris et al. 2007) and validated by field capacity and percolation coefficient equation (Louloudis et al. 2022) in the Ptolemais area. It is worth mentioning that remote sensing technology has made remarkable advancements over the years, enhancing the previous indices and their critical evaluation. Moreover, satellite imagery has undergone notable improvements, including the enhancement of spatial resolution and the provision of data without the need for extensive pre-processing (Table 3).

Finally, the flood risk was estimated for the areas using most of the aforementioned indices. Specifically, eight flood conditioning parameters, namely, DEM, slope, rainfall, distance from the main river, *TWI*, land use/ land cover, *RIP*, and *NDVI* were selected and converted into fuzzy values, using the following fuzzy function in a GIS environment:

$$f(x) = \begin{cases} 1, if\ x > x_{max} \\ 0,\ if\ x < x_{min} \\ (x - x_{min})/(x_{max} - x_{min}),\ if\ x_{min} < x < x_{max} \end{cases}$$

where x_{max} and x_{min} depict the maximum and minimum values of each parameter and x represents each pixel value parameter. Moreover, the value of "0" corresponds to areas with a low risk of flooding, while "1" corresponds to areas with a high risk. Consequently, maps presenting a range of 0–1 were produced for each of the indices, which were subsequently classified in the GIS environment by using specific weight factors w_i, determined via the analytic hierarchy process (AHP) (Parsian et al. 2021), which are provided in Table 4.

Subsequently, the fuzzy gamma operator was introduced in the GIS environment as an algebraic product of the fuzzy product and fuzzy sum function, both raised to the power of gamma (γ), aiming to integrate all of the parameters and develop the final fuzzy flood hazard map F(γ). The following transformation function was used, where n corresponds to each parameter and $f(i)$ is the pixel value in each parameter map, while considering the literature (Esmaili and Taheri 2022; Parsian et al. 2021). A γ value above 0.70 can show higher accuracy:

$$F(\gamma) = \prod_{i=1}^{n} f(i)^{1-\gamma} \left(1 - \prod_{i=1}^{n} (1 - f(i))\right)^{\gamma}$$

The final flood susceptibility map was produced by applying the GIS natural breaks (Jenks) operator, where classification was conducted, and pixels of similar values were

Table 4 Weight factors applied individually to each main parameter, estimated from the Analytic Hierarchy Process (AHP)

Parameters	Weight (%)
DEM	16.2
Slope	12.4
Rainfall	18.4
Distance from the main river	19.5
TWI	2.7
Land use/ Land cover [1]	13.9
RIP	7.4
NDVI	9.5
Total	100

[1]Source: Corine Land Cover (Copernicus, https://land.copernicus.eu/pan-european/corine-land-cover) for the area outside the mine boundary and PPC data for the area inside this boundary

grouped to maximize the differences between the classes. The produced flood hazard susceptibility presented five classes (very low, low, moderate, high, and very high) to delineate the areas more susceptible to flooding.

In Fig. 6, the methodological approach is presented briefly to illustrate the modelled processes. First, the data was collected and pre-processed for our study area. This procedure was done mostly by the data collector and includes atmospheric correction and reduction of air molecule scattering. After that, the data was adjusted for the study area. The specific dates of the images were chosen based on the season and clarity. Moreover, the meteorological data was based on the eight meteorological stations near the mine activity. Subsequently, the topographic and spectral indices were produced and evaluated as well as the rainfall grid and the infiltration coefficient. Consequently, several indices were selected, and weight factors assigned by using the AHP to identify the flood susceptible areas. It is worth mentioning that the indices *NDWI*, *MNDWI*, *SPI*, and *LS* were not selected because they generated a deflection between the susceptibility maps and the recorded flood events. Furthermore, the *NDWI* and *MNDWI* indices are subject to uncertainties due to climatological conditions and the *LS* and *SPI* indices have very low values and thus cannot affect the results in the area of interest. However, the potential contribution of these indices in the comprehension of the hydrologic status is very essential. Finally, the fuzzy membership method was used to transform the input data into the 0 and 1 scale. All the data was input into the fuzzy overlay tool where the flood susceptibility maps were produced.

Results and Discussion

The study area is dominated by the small water bodies and low-flowing streams that are the main surface water sources in the research region (Fig. 1). The maps created using the topographic and spectral indices identify the water bodies in the area. Regarding the appearance and location of these water bodies, the results are in line with prior studies, i.e. the topographical mapping carried out by PPC for the area inside the boundary of mining activities and the Hellenic Military Geographical Service for the broader area of research (Table 1).

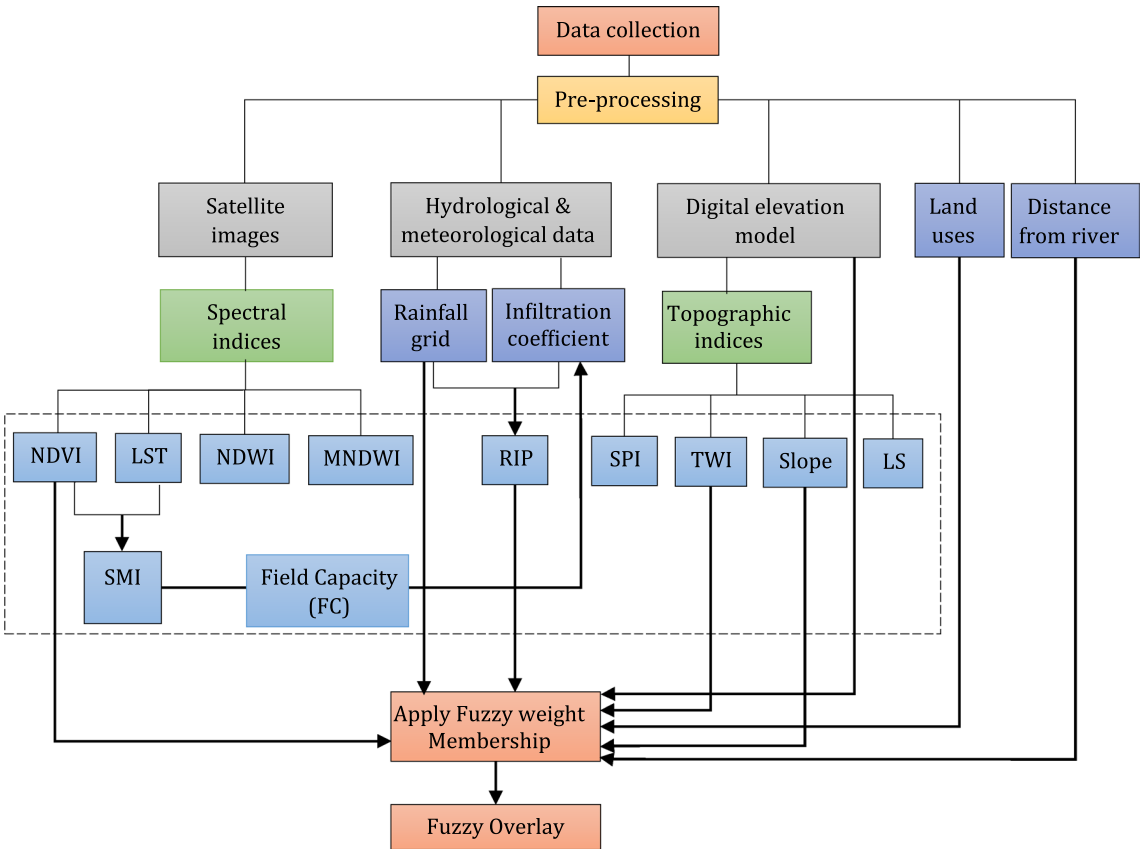

Fig. 6 Flowchart of the methodological approach

The water-saturated areas are depicted where the relative wetness in catchment areas is predicted by the spatial dist,ribution of the *TWI* (Fig. 7) and *SPI* (Fig. 8.) indices. These figures show that there are small areas inside the boundary of mine activity where water flow is concentrated. Also, the drainage basin is evident. In particular, the spatial distribution of the *TWI* values show the water accumulation trend towards a location, due to how the slope affects hydrological processes. The drainage channels developed inside the boundary of mine activities are evident. Water is also concentrated in the Sarigiol basin, as shown in the *TWI* distribution map, and more specifically south of the South Field lignite mine, where low *SPI* values were calculated, indicating the low erosive power of the flowing water. It is apparent that the drainage channels developed through the *TWI* index align with the hydrographic network previously recorded by PPC's geologists conducting field research (Fig. 2).

The spatial distribution of the *SPI* shows high values in the northeast and south-southwest areas of mining activity, where the water runoff and overland flow of the Vermion, Askion, and Skopos Mts. are active. The results delineate areas where the erosive power of the streams is high due to surface runoff. Additionally, the distribution of *LS* values (Fig. 9) indicates that water discharge is evident only in the mountains. At the same time, lower calculated values are scattered inside the boundary of the mining activity and in the agricultural area outside the mines. An important issue is the intensity of weathering, which is more pronounced around Vermion Mtn. Erosion plays a crucial role in identifying regions susceptible to flooding processes where weathered materials are eventually deposited in water bodies, increasing the threat of overflowing.

Our results suggest that the potential for hydrologically active streams is greater near Vermion Mtn. than Askion Mt. Soulou River and its channels appear more active, presenting perennial flow. Our findings reveal the tendency of surface runoff, where intermittent flow is evident northeast of the South Field external waste dumping area and the area of waste dumping inside the mines. High flow velocities are evident only in outcropping bedrock areas like the mountainous regions.

Subsequently, water-stressed conditions were evaluated using spectral indices. In the research area, *NDVI* (Fig. 10) was calculated for the dry period of the summer season. The summer season indicates the growing season with the maximum vegetative coverage in the area by the "greenness" of the image. Typically, high *NDVI* values illustrate younger and more healthy vegetation, while low values correspond

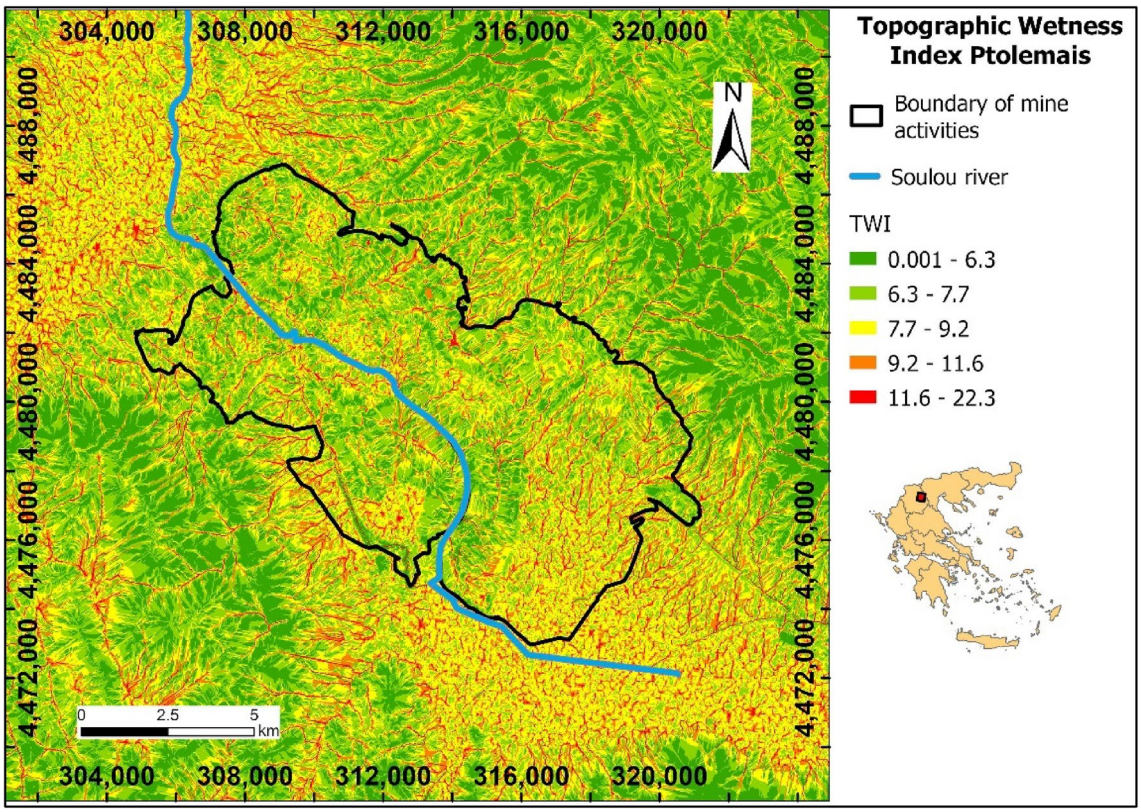

Fig. 7 Spatial distribution of *TWI* with the combinations of two DEMs in 2022 where drainage networks are shown in red colour, (Ptolemais Basin, northern Greece). The area of mining activities is indicated in black

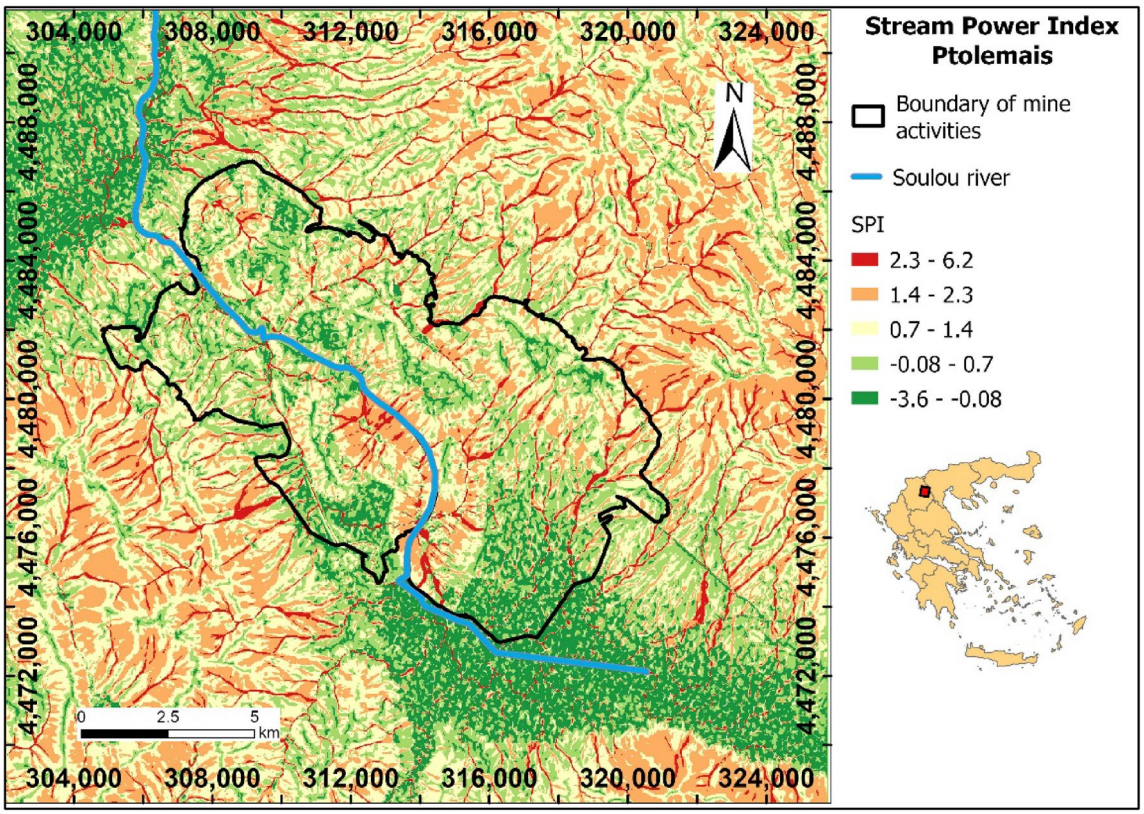

Fig. 8 Spatial distribution of *SPI* with the combinations of two DEMs in 2022 where high velocity of the streams is presented with red values (Ptolemais Basin, northern Greece). The area of mining activities is highlighted in black

to a lack of vegetation. According to Fig. 10, the area of the outside waste dumping, i.e. the northern of the South Field Lignite mine, has a vegetative cover due to the mine restoration activities. Strong evidence of young and healthy vegetation also appears in the cultivated agricultural land, as shown in the southern area of the South Lignite Mine.

Additionally, *NDWI* and M*NDWI* indices were produced for the same area in the wet season when high rainfall and very little green vegetation occurred. Even though *NDWI* can successfully improve information on water occurrence at the surface, it is sensitive to built-up terrain, and is unable to discriminate forests and grassland from true surface water occurrences. To address this problem, the M*NDWI* index (Xu 2006) is calculated, which enhances the contrast between water features and areas with built-up land, soil, and vegetation.

In Fig. 11A, the *NDWI* map shows the water features, enhancing their presence. The spatial distribution of the *NDWI* values delineate water accumulation in locations with a high potential for inundation. The contrast between water features and other land surface features is further enhanced in the M*NDWI* map (Fig. 11B).

The spatial distribution map of M*NDWI* values is produced for the same area and the same satellite image, but with the noise from the urban areas (see Fig. 1) minimized or removed. The findings of M*NDWI* and *NDWI* processing are consistent with the satellite images. Specifically, high index values > 0.90 represented by dark blue colours appear in the northeast area of the Vermion Mtn, range due to the snow coverage as the satellite image was taken in December. Similar high index values > 0.90 appear in the southwest area of Askion Mtn. with high stream runoff rates along the slopes of the mountain range (Fig. 2). Further apparent dark blue features within the mining area in the M*NDWI* map correspond to the location of the mine sumps.

Subsequently, *SMI* spatial distribution map was produced based on the calculated *NDVI* spatial distribution combined with the surface temperature using Landsat 8 OLIS/TIRS satellite data (Fig. 12). The data highlights the temperature distribution during July 2022, so high temperatures are observed inside the mine sites. The mean temperature value was 34 °C, while the temperature recorded at that time ranged from 9 to 45 °C. After calculating the spatial distribution of the temperature, a regression model was used to find the values of LST_{MAX} and LST_{MIN}. The *SMI* spatial distribution was calculated empirically based on the scatter diagram of *LST* and *NDVI* values.The distribution usually shows a trapezoidal or triangular shape (Sandholt

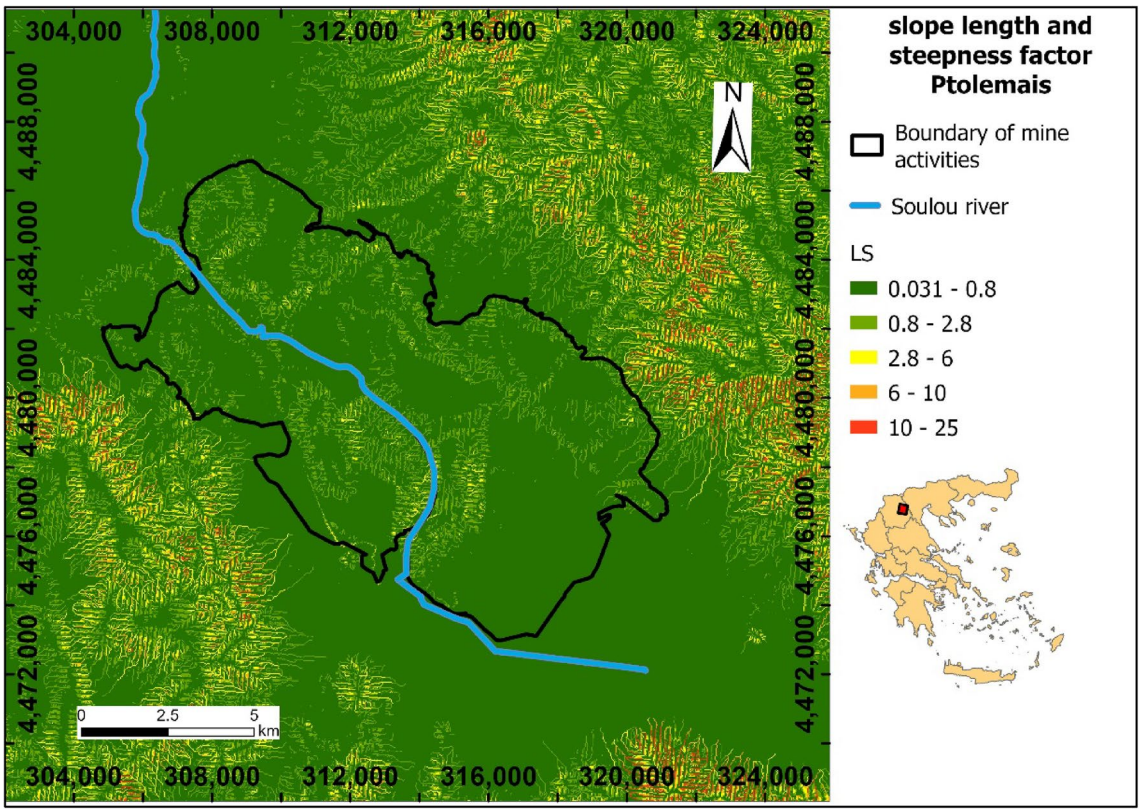

Fig. 9 Spatial distribution of *LS* where high erosion is indicated by red colour (Ptolemais Basin, northern Greece). The area of mining activities is shown in black

et al. 2002). Furthermore, only the values exceeding 0 were selected, which marks the limit of vegetation coverage. In Fig. 13, the regression results are documented using a scatter plot.

The mapped *SMI* distributed values (Fig. 14) illustrate spots of high soil moisture values (the blue areas), in the areas outside the mine, representing agricultural land cover. Irrigation of agriculture is common during the summer months. The area outside of the waste rock dumping, i.e., north of the South Lignite Field and within the boundary of mining activities, also has high soil moisture. This is due to small forests as land cover, which were build up over the past years of reclamation activities.

The final index that was calculated from the satellite imagery is *RIP*, which describes the percentage of precipitation that can potentially infiltrate the rock strata and contribute to groundwater recharge. To calculate the index, the average annual precipitation and the estimated infiltration coefficients of the lithology were considered. Average annual precipitation was calculated based on data from the meteorological stations in the area. Subsequently, the regression between the average annual precipitation and the elevation was calculated to create the rainfall grid.

The annual average precipitation is depicted (Fig. 15) and exhibit lower values inside the area of mining activities and in the agricultural fields compared to higher values at higher elevations in the mountainous areas (see Fig. 1). The raster map was derived from the correlation of the elevations and average annual precipitation at different meteorological stations (Fig. 16), while the data were obtained from the National Observatory of Athens (NOA) (https://meteo.gr/Gmap.cfm). The illustration also shows the station locations within the research area. Note that the meteorological stations depicted in Fig. 16 are all less than 14 km from our designated study area.

The spatial distribution of the *RIP* index was calculated by multiplying the rainfall grid and the infiltration coefficients. According to the results (Fig. 17), the RIP values are generally higher in the mountain ranges consisting of karstic limestones (see Fig. 2), which exhibit high permeability. Low RIP values are indicative of waste dump areas and the area of the Sarigiol basin due to the high percentage of impermeable fine-grained sediments, mainly of silt- and claystones. Similar low values are evident for the excavated areas inside the open pit mines, as the average annual precipitation generates low values, the formed slopes exhibit

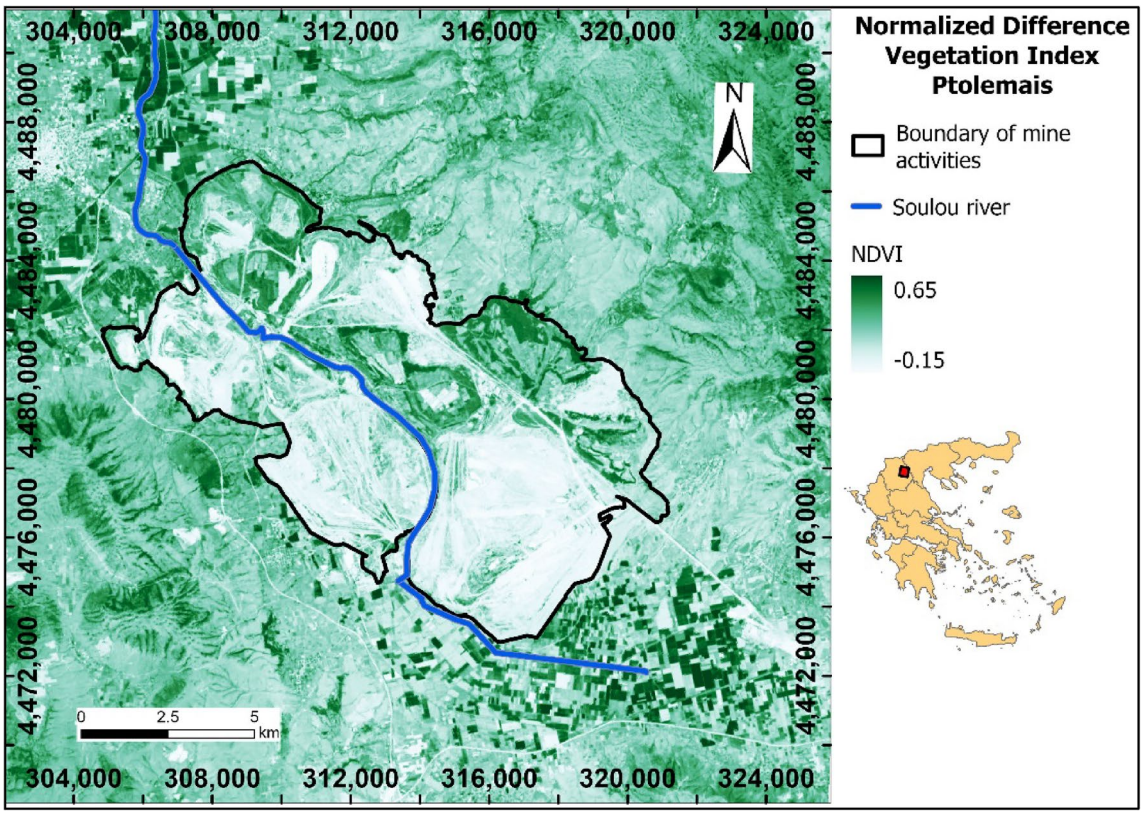

Fig. 10 Spatial distribution of *NDVI* in July 2022 (Ptolemais Basin, northern Greece). Higher values of *NDVI* suggest healthy and dense vegetation while lower values non-vegetated-surfaces

high inclinations, and the impermeable surface materials favour surface runoff.

The flood susceptibility map summarizes most of the aforementioned indices (Fig. 18). A fuzzy logic function overlay was employed on a GIS map to determine the locations susceptible to flooding. Based on the proposed methodology, the maps produced in Fig. 18 present five classes delineating the areas with very high, high, moderate, low, and very low susceptibility to flooding. The map was produced considering gamma values of γ=0.80 (Fig. 18A) and γ =0.90 (Fig. 18B) to evaluate the sensitivity of this parameter.

The visualization of the flood susceptibility maps produced satisfactory results for both gamma values. The results indicated that the likelihood of potential flooding is increased inside the boundary of the mining activities, especially within the open pits. In contrast, the areas with very low risk of flooding are the restored areas of the external waste dump (the northern portion of the exploitable lignite deposits). Moreover, the agricultural areas outside the area of mining activities show moderate to high susceptibility to flooding. The two Fig. 18 maps, showing the relative potential flood risk are compared in Tables 5 and 6**.** This comparison shows a very similar distribution of flood risk between the two maps.

Based on the PPC flood event reports during heavy rainfall and also events reported in the National River Basin Management Plans (https://floods.ypeka.gr), flooded locations were observed in the old Sarigiol swamp (the area south and southwest of the exploitable lignite deposits), where drainage canals are used to transfer water to the agricultural area for irrigation. Also, a flood event is recorded in the deepest sump inside the South Field Lignite mine, as is delineated in the *NDWI* and *MNDWI* spatial distribution maps. Based on the flood event recordings, the obtained results are in line with observations and yield an accurate flood susceptibility map. Furthermore, the proposed approach provides new insight into integrated land use planning for large-scale areas, where remote sensing data combined with the geographical information system (GIS) could feature detailed spatiotemporal information, –supporting a pre-assessment of potential water hazards like flood occurrence.

Based on the results of this study, the area inside the surface lignite mines, is characterized by high values of *TWI*

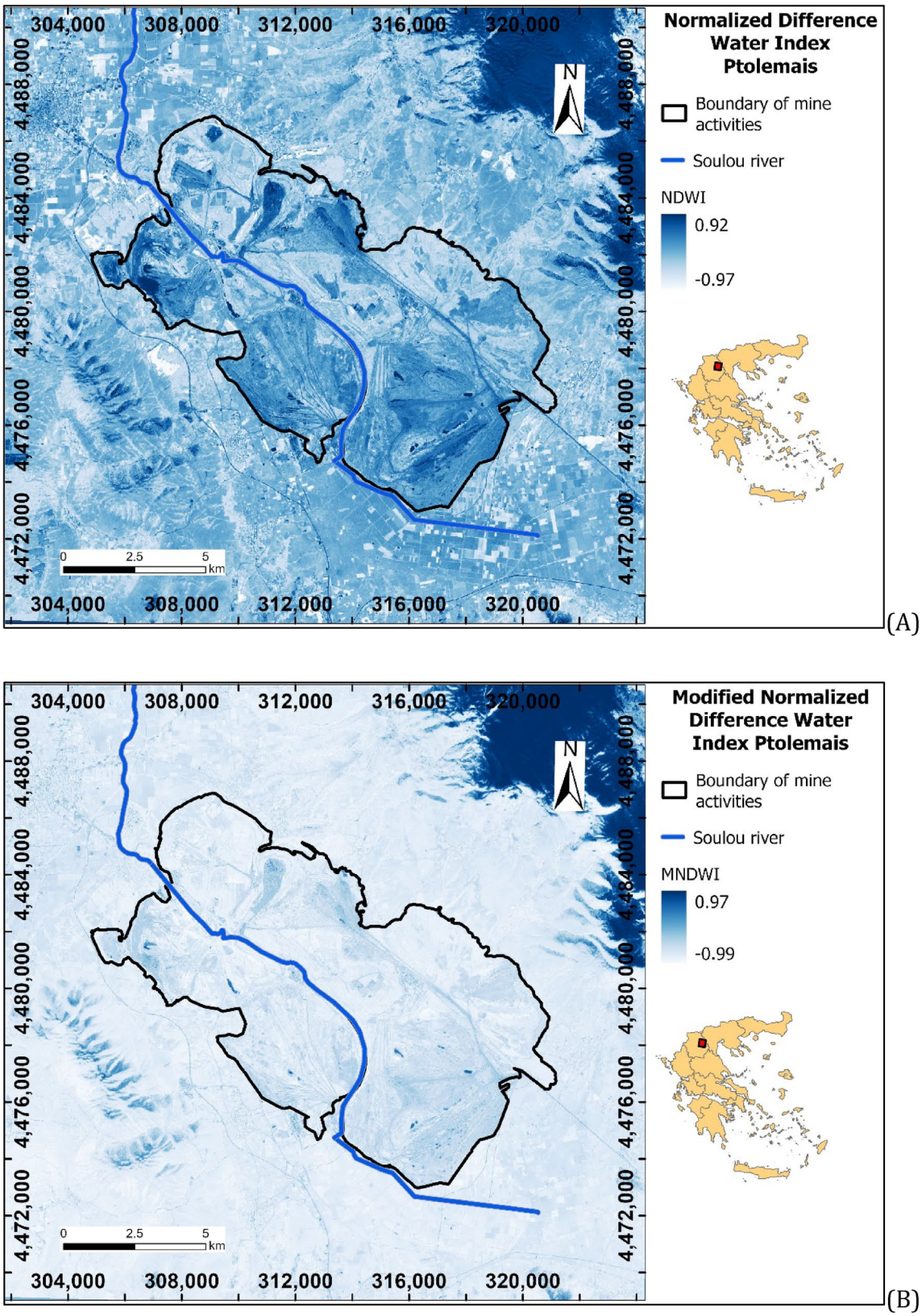

Fig. 11 Spatial distribution map of *NDWI* (**A**) and *MNDWI* (**B**); indices ranging from + 1 to −1 recorded in December 2021 (Ptolemais Basin, northern Greece). Water features are represented by dark blue colour. The area of mining activities is outlined as black line

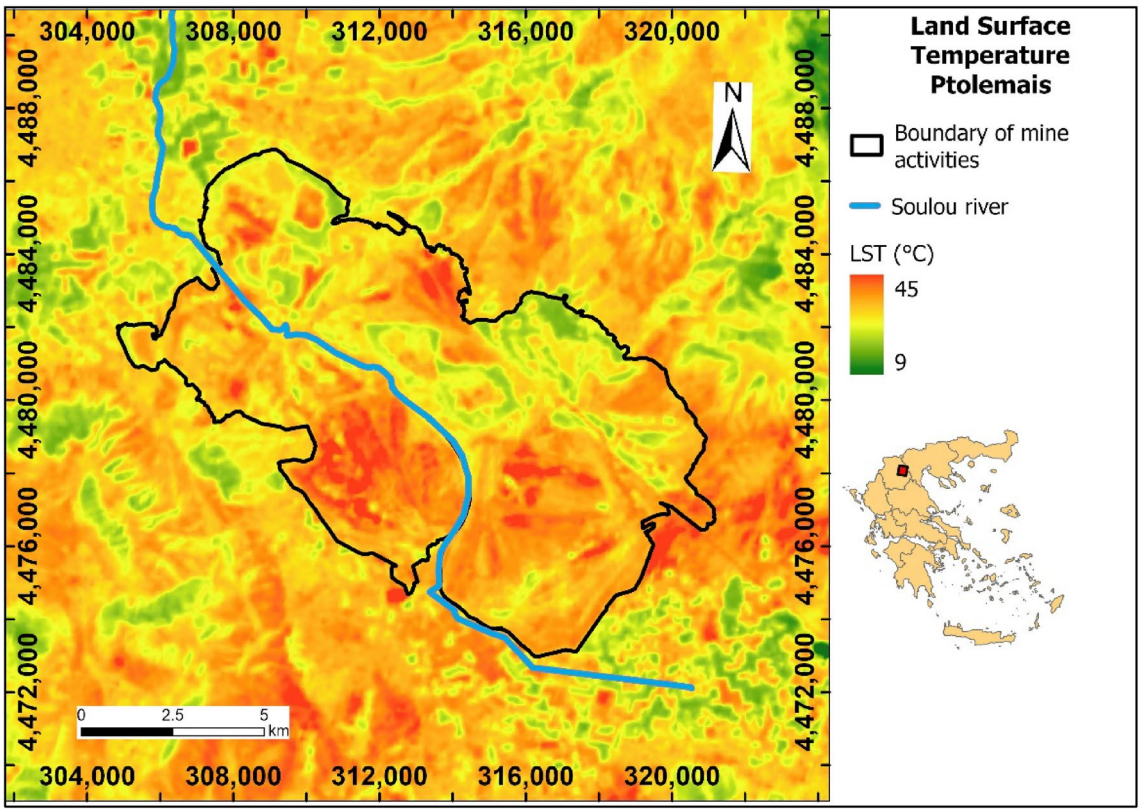

Fig. 12 Spatial distribution of temperature in July 2022(Ptolemais Basin, northern Greece). The area of mining activities is shown

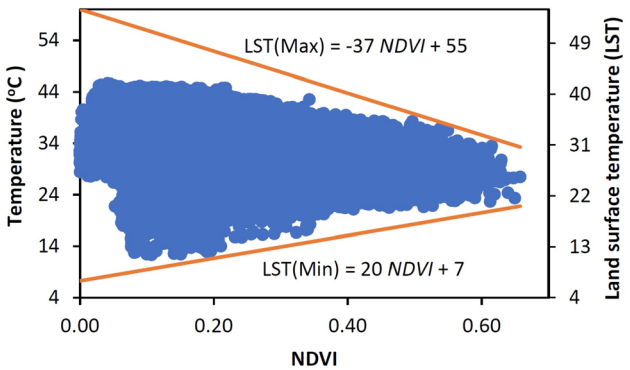

Fig. 13 Scatter plot of land surface temperature (*LST*) vs *NDVI* in July 2022 (Ptolemais Basin, northern Greece)

where the water flow is concentrated. On the other hand, concerning infiltration potential inside the open pits, low *RIP* values are generally calculated, while based on the flood susceptibility map produced, these areas are more likely to flood. In addition, low to moderate values of *SMI* are calculated, except for the areas of mine sumps where high values are evident.

Within the inside dumping areas, high to moderate values of *SPI* and *LS* are derived, where the erosive power of water flow is high due to surface runoff. Additionally, high values of *SPI* and *LS* are apparent in the west foothills of Vermion Mt., along the transition of consolidated and unconsolidated sediments of the east margins of Sarigiol basin. This confirms the thesis that a great portion of clastic ophiolithic materials is transferred from Vermion Mt. to Sarigiol basin (Vasileiou et al. 2019).

The external waste dump area is characterized by moderate *LS* values scattered about this area, which marks its intensity of weathering, and subsequently an increased potential for local flooding, as indicated in the produced flood susceptibility map. This specific index will have lower values in the future if the conversion of mine sites to new land uses like the development of photovoltaic parks or forested areas considers the findings of this study to reduce the weathering potential.

Based on the produced flood susceptibility maps, the restored areas of the external waste dump (the northern portion of the exploitable lignite deposits) have very low risk, while the areas that are prone to flooding are the open pits and the areas of the waste dumps deposits that are not restored yet. The areas outside the boundary of the mining

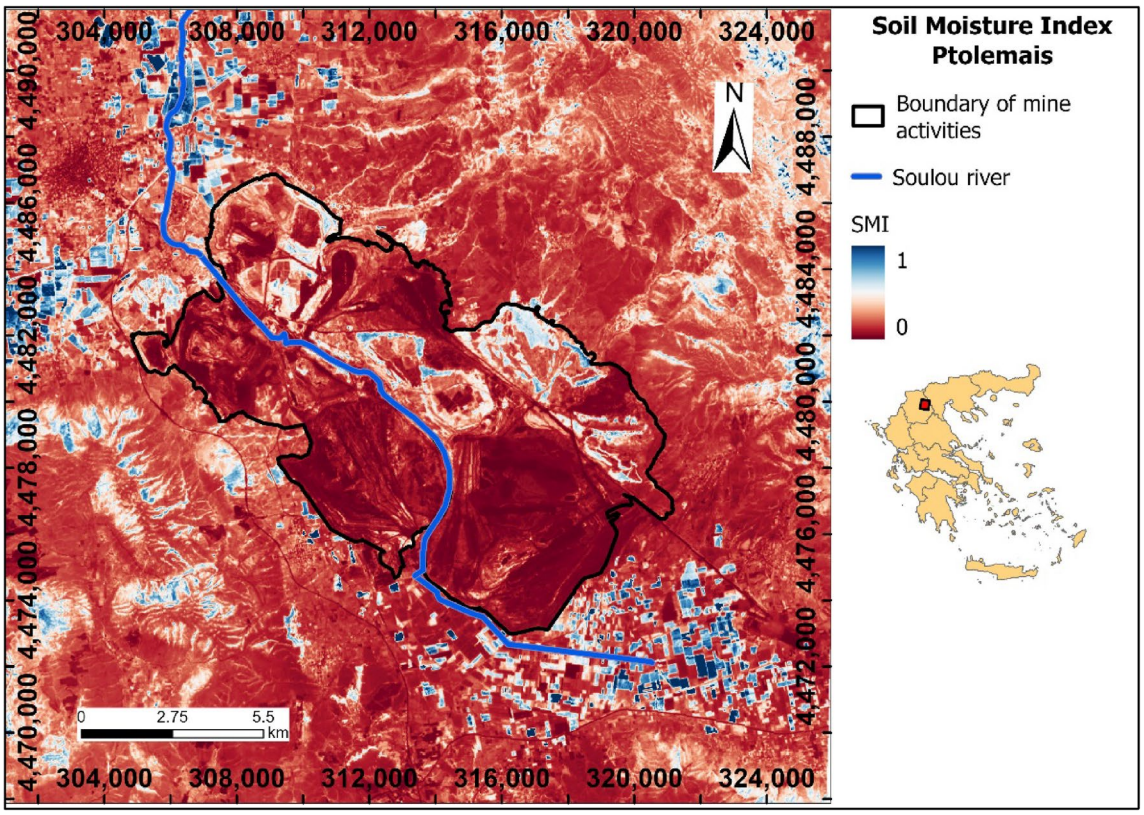

Fig. 14 Spatial distribution of *SMI* in July 2022 (Ptolemais Basin, northern Greece), where high soil moisture values are indicated by blue colour, representing agricultural fields and forests. The area of mining activities is shown

Table 5 Areas prone to flooding inside the boundary of mine activities, in the Ptolemais Basin, northern Greece

Gamma value (γ)	Areas susceptible to flooding (%)				
	Very low susceptibility	Low susceptibility	Moderate susceptibility	High susceptibility	Very high susceptibility
0.90	15	1	11	28	45
0.80	15	1	11	30	43

Table 6 Areas prone to flooding outside the boundary of mine activities and inside the watershed, in the Ptolemais Basin, northern Greece

Gamma value (γ)	Areas susceptible to flooding (%)				
	Very low susceptibility	Low susceptibility	Moderate susceptibility	High susceptibility	Very high susceptibility
0.90	55	6	25	10	4
0.80	56	6	26	9	3

activities are characterized by very low to moderate flood risk, except for the urbanized areas where the flood susceptibility is very high. Tables 5 and 6 offer an improved understanding of the hydrological attributes of the Ptolemais Basin and indicate that more regions within the area of mining activity are susceptible to flooding than outside the boundary.

Conclusions

The main objective of this research was to develop a methodology to evaluate the surface water hydrology in a large and complex area, like a surface mining site. The rapidly changing energy situation based on the transition away from fossil fuels in Greece, with the closure of lignite mines in progress and post-mining repurposing scenarios to be planned, is rather challenging for land use planning and resource allocation. Therefore, the research focused on a hydrological confined basin, investigating the use of remote sensing and topographic data for the Ptolemais Basin in western Macedonia, Greece. In general, the use of remote sensing data and the study of the topographic profile of an area could provide a very coherent estimation of its surface water based

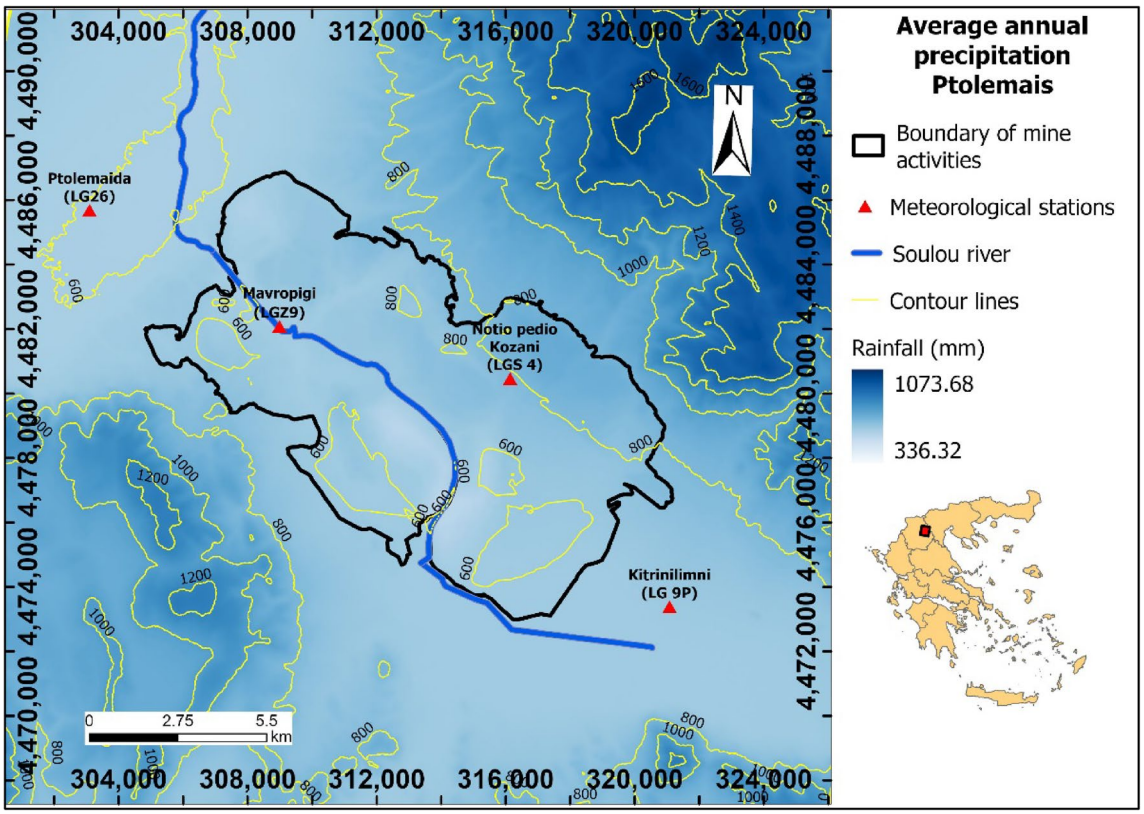

Fig. 15 Spatial distribution of average annual precipitation (Ptolemais Basin, northern Greece). The area of mining activities is shown in black

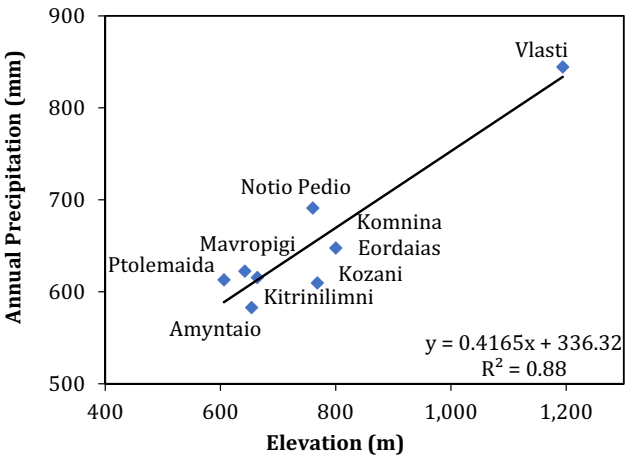

Fig. 16 Correlation of annual precipitation and elevation in the Ptolemais Basin, northern Greece. Eight meteorological stations were considered indicated in blue colour

hydrological character, which is a key factor influencing future land use structure. Additionally, meteorological data predictions and climatic change should also be considered, as these factors influence the hydrology of an area.

The applied methodology also permitted sufficiently accurate mapping of hydrological characteristics derived from various indices of satellite imageries in the large and complex mining area of the Ptolemais Basin. Specifically, satellite images and topography provided details of the surface water hydrology, which helped identify challenges that must be faced for effective land use planning. Water bodies, low-flowing streams, and water flow directions were identified, covering the main surface water sources in the research region. The most erodible areas were also evident, which was vital in delineating areas where weathered materials were deposited. Subsequently, water accumulation was outlined in specific locations where there was high potential for inundation. The integration of vegetative cover and surface temperature proved to be valuable for mapping the soil moisture of the research area.

Traditional modelling has focused on the temporal dynamics of a specific area. However, spatiotemporal evaluation using high-resolution data can provide a more realistic approach and more reasonable outputs. The methodology proved to be sufficiently robust to evaluate surface water features in large complex areas, like surface mining sites. In addition, this methodology proved capable of evaluating potential hazards, like areas that are susceptible to flooding. In the examined case study, areas with a potential flood risk were delineated, using remote sensing data to produce flood susceptibility maps. The results correlated well with

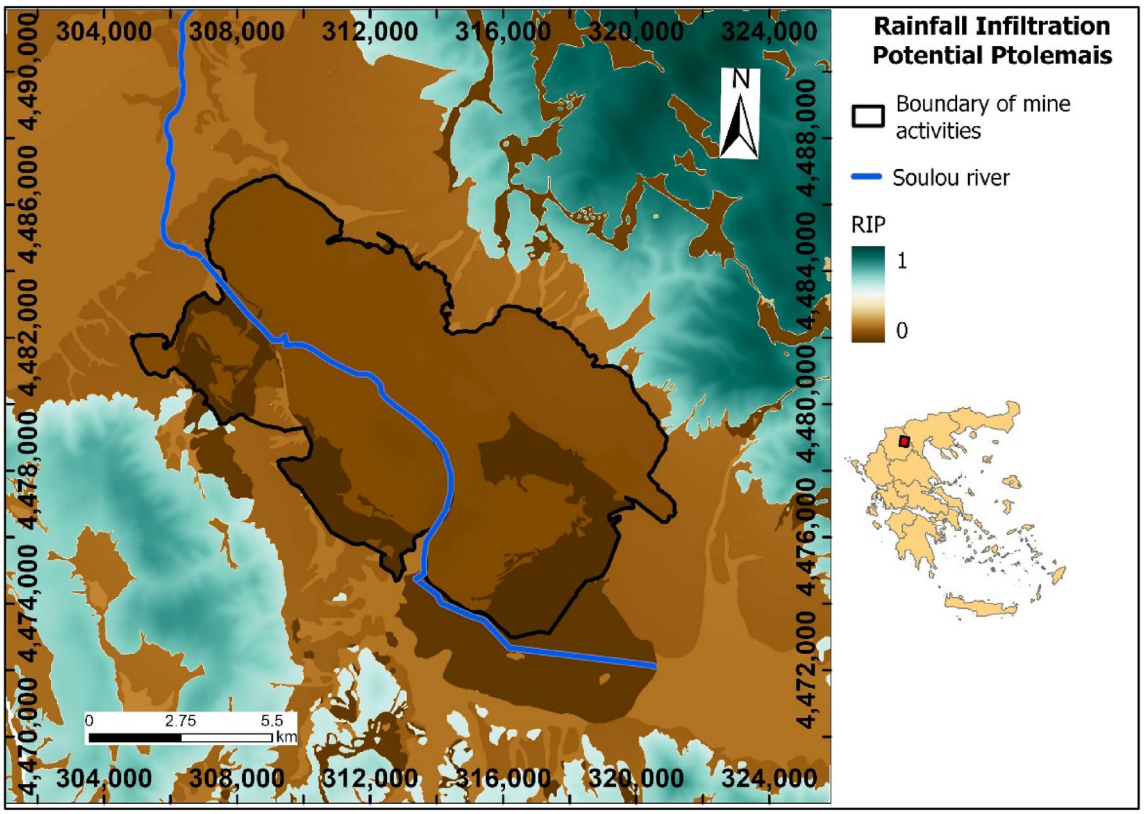

Fig. 17 Spatial distribution of *RIP* in the Ptolemais Basin, northern Greece. The area of mining activities is shown

recorded flood events, demonstrating the high potential of the approach for creating an accurate flood susceptibility map. Based on the results, the areas outside the boundary of the mining activities present very low to moderate risk; therefore, small, local water management infrastructure is considered more appropriate than large-scale surface hydraulic protective measures.

The proposed approach provides new insight into integrated land use planning for large-scale areas. Remote sensing data combined with GIS could feature detailed spatiotemporal information, helping evaluate spatial patterns of different hydrological features. The dynamic relationship between these features and land use patterns could help effective strategic planning and, thus, successful and efficient mine reclamation. Furthermore, considering the analysis and evaluation of various reclamation options and making decisions about post-mining future and economic transitions, this methodology could lead to recognising potential hazards in the surrounding region, defining possible barriers such as zones with a very high susceptibility to flooding, thus contributing effective land use planning and new and improved water management strategies. Thus, we strongly recommend using remote sensing data and high-resolution DEM to implement an integrated approach for evaluating large areas based on suitability criteria for different land uses.

Aims for future research include analysing remote sensing data to delineate flooded areas on specific dates when

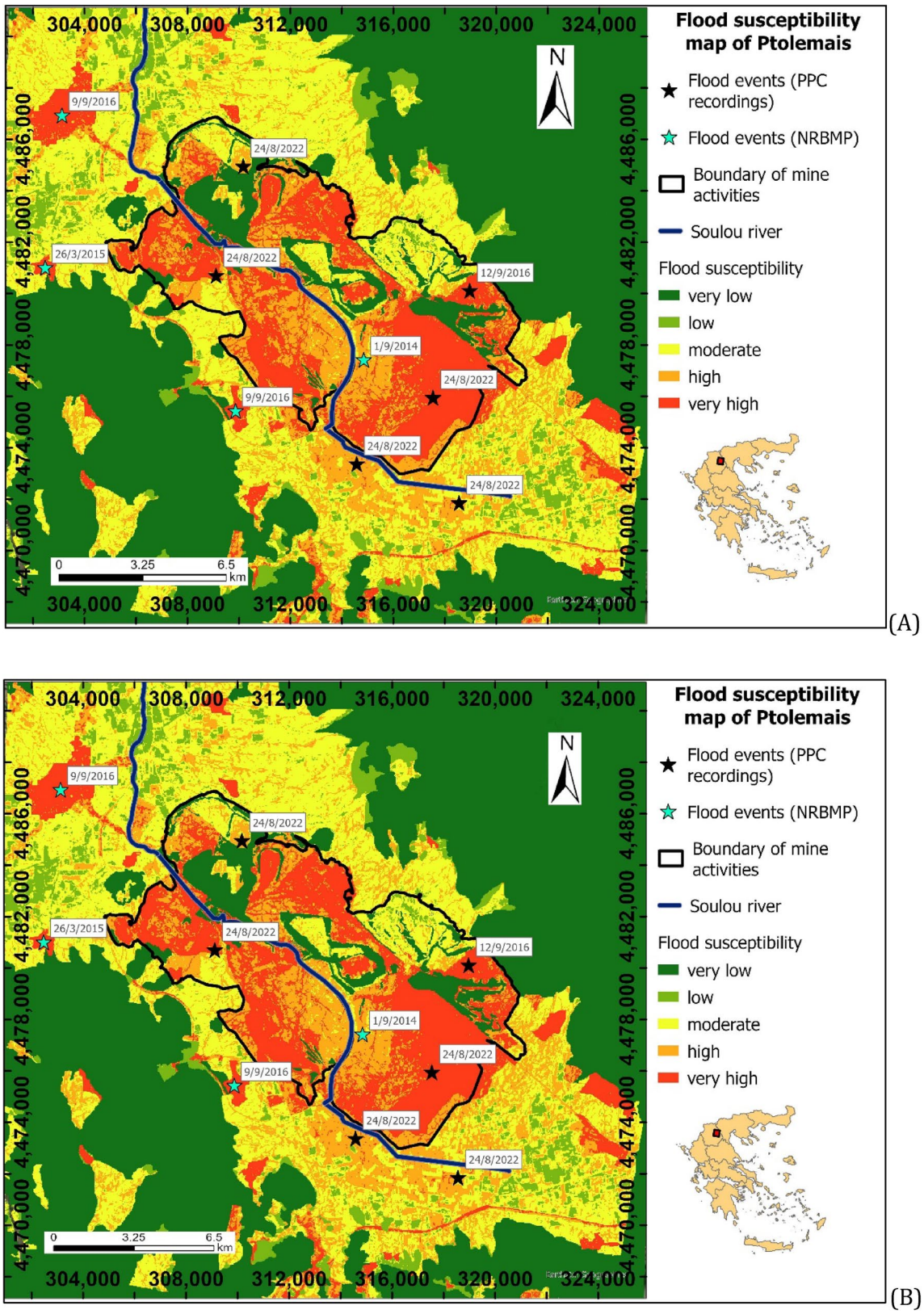

Fig. 18 Zones prone to flooding, (Ptolemais Basin, northern Greece), the area of mining activities is shown in black. **A** Gamma value $\gamma = 0.80$ and, **B** gamma value $\gamma = 0.90$ using fuzzy gamma overlay in GIS environment. Flood events are presented based on the PPC Flood Event Reports and the National River Basin Management Plans (NRBMP, https://floods.ypeka.gr)

extreme weather conditions and heavy rains occur. Thus, the methodology proposed to forecast the zones prone to flooding would be further validated by comparison with flood detection using satellite data. By incorporating an assessment of flood-prone areas into the decision-making process, PPC could form potential strategic frameworks for land reclamation and environmental remediation. These strategies are intended to mitigate the risk of flooding and provide sustainable post-mining land uses.

Data availability Data will be made available by the authors upon request.

References

Acharya T, Lee D, Yang I, Lee J (2016) Identification of water bodies in a Landsat 8 OLI image using a J48 decision tree. Sensors 16:1075. https://doi.org/10.3390/s16071075

Berg A, Sheffield J (2018) Climate change and drought: the soil moisture perspective. Curr Clim Change Rep 4:180–191. https://doi.org/10.1007/s40641-018-0095-0

Beven KJ, Kirkby MJ (1979) A physically based, variable contributing area model of basin hydrology / Un modèle à base physique de zone d'appel variable de l'hydrologie du bassin versant. Hydrol Sci Bull 24:43–69. https://doi.org/10.1080/02626667909491834

Buchanan BP, Fleming M, Schneider RL, Richards BK, Archibald J, Qiu Z, Walter MT (2014) Evaluating topographic wetness indices across central New York agricultural landscapes. Hydrol Earth Syst Sci 18:3279–3299. https://doi.org/10.5194/hess-18-3279-2014

Byrne K (2018) Digital morphometry applied to geo-hazard risk assessment: a case study from Germany. PhD Diss, Technical Univ of Dresden

Caturegli L, Matteoli S, Gaetani M, Grossi N, Magni S, Minelli A, Corsini G, Remorini D, Volterrani M (2020) Effects of water stress on spectral reflectance of bermudagrass. Sci Rep 10:15055. https://doi.org/10.1038/s41598-020-72006-6

Copernicus (2023) Sentinel-2 MSI (User Guide). https://sentinels.copernicus.eu/web/sentinel/user-guides/sentinel-2-msi/processing-levels/level-2. Accessed 26 June 2022

Danielson T (2013) Utilizing a high resolution digital elevation model (DEM) to develop a stream power index (SPI) for the Gilmore Creek watershed in Winona County, Minnesota. St Mary's Univ Minn Univ Cent Serv Press Winona MN 15:11

Dimitrakopoulos D, Grigorakou E (2004) Aquatic balance of Vegoritis Lake, West Macedonia, Greece, related to mining activity. In: Jarvis AP, Dudgeon BA, Younger PL (eds), Proc, Mine Water 2004—International Mine Water Assoc Symp, pp 201–207

Esmaili R, Taheri M (2022) Evaluation of flood hazards areas with fuzzy approach, case study: downstream of Neka catchment, Mazandaran Province. J Nat Environ Hazards 11(34):145–158. https://doi.org/10.22111/jneh.2022.39817.1842

European Commission, Directorate-General for Environment (2021) The 6th Water Framework Directive and Floods Directive Implementation Report. Publications Office of the European Union, Brussels, Belgium. https://environment.ec.europa.eu/publications/6th-water-framework-directive-and-floods-directive-implementation-report_en. Accessed 20 Jun 2022.

Ghunowa K, MacVicar BJ, Ashmore P (2021) Stream power index for networks (SPIN) toolbox for decision support in urbanizing watersheds. Environ Model Softw 144:105185. https://doi.org/10.1016/j.envsoft.2021.105185

Gomis-Cebolla J, Garcia-Arias A, Perpinyà-Vallès M, Francés F (2022) Evaluation of Sentinel-1, SMAP and SMOS surface soil moisture products for distributed eco-hydrological modelling in Mediterranean forest basins. J Hydrol 608:127569. https://doi.org/10.1016/j.jhydrol.2022.127569

Government Gazette 2689/B/6.07.2018 (2018) Approval of Flood Risk Management Plan of the West Macedonia River Basin District (EL 09). Decision no. ΥΠΕΝ/ΓρΕΓΥ/41387/331

Government Gazette 4676/B/29.12.2017 (2017) Approval of the 1st Revision of River Basin Management Plan of the River Basins of Western Macedonia River Basin District (EL09). Decision no. οικ.906

Jacoby BS, Peterson EW, Dogwiler T (2011) Identifying the stream erosion potential of cave levels in Carter Cave State Resort Park, Kentucky, USA. J Geogr Inf Syst 03:323–333. https://doi.org/10.4236/jgis.2011.34030

Kopecký M, Macek M, Wild J (2021) Topographic Wetness Index calculation guidelines based on measured soil moisture and plant species composition. Sci Total Environ 757:143785. https://doi.org/10.1016/j.scitotenv.2020.143785

Koukouzas N, Ward CR, Li Z (2010) Mineralogy of lignites and associated strata in the Mavropigi field of the Ptolemais Basin, northern Greece. Int J Coal Geol 81:182–190. https://doi.org/10.1016/j.coal.2009.12.012

Lakshmi V (2015) Remote sensing of the terrestrial water cycle. American Geophysical Union, Wiley, Hoboken

Liang D, Lu J, Chen X, Liu Ch, Lin J (2020) An investigation of the hydrological influence on the distribution and transition of wetland cover in a complex lake–floodplain system using time-series remote sensing and hydrodynamic simulation. J Hydrol 587:125038. https://doi.org/10.1016/j.jhydrol.2020.125038

Louloudis G, Roumpos C, Louloudis E, Mertiri E, Kasfikis G (2022) Repurposing of a closed surface coal mine with respect to pit lake development. Water 14:3558. https://doi.org/10.3390/w14213558

Louloudis G, Stathopoulos N (2019) Irrigation water consumptive use changes in south Ptolemais lignite bearing hydrogeological basin (Greece) using NDVI remotely sensed data. In: Kranis H (ed), Proc, 15th International Congress of the Geological Soc of Greece. Bull Geol Soc Greece, pp 611–612

Louloudis G (1991) Hydrogeological conditions of south lignite bearing field of Ptolemais region. Confrontation of groundwater problems during the exploitation. PhD Diss, Natl Tech Univ Athens, Sch Min Metall Eng [in Greek]

McFeeters SK (1996) The use of the normalized difference water index (NDWI) in the delineation of open water features. Int J Remote Sens 17:1425–1432. https://doi.org/10.1080/01431169608948714

Meles MB, Younger SE, Jackson CR, Du E, Drover D (2020) Wetness index based on landscape position and topography (WILT): Modifying TWI to reflect landscape position. J Environ Manage 255:109863. https://doi.org/10.1016/j.jenvman.2019.109863

Mendiguren G, Koch J, Stisen S (2017) Spatial pattern evaluation of a calibrated national hydrological model—a remote-sensing-based diagnostic approach. Hydrol Earth Syst Sci 21:5987–6005. https://doi.org/10.5194/hess-21-5987-2017

Modis K, Sideri D, Roumpos C, Binet H, Pavloudakis F, Paraskevis N (2022) Geostatistical modeling of overburden lithofacies to optimize continuous mining in the Ptolemais lignite mines. Greece Minerals 12:1109. https://doi.org/10.3390/min12091109

Moore ID, Burch GJ (1986) Physical basis of the length-slope factor in the universal soil loss equation. Soil Sci Soc Am J 50:1294–1298. https://doi.org/10.2136/sssaj1986.03615995005000050042x

Moore ID, Wilson JP (1992) Length-slope factors for the revised universal soil loss equation: simplified method of estimation. J Soil Water Conserv 47:423–428

Moore ID, Grayson RB, Ladson AR (1991) Digital terrain modelling: a review of hydrological, geomorphological, and biological applications. Hydrol Process 5:3–30. https://doi.org/10.1002/hyp.3360050103

Papakōnstantinu A (1979) Die hydrogeologischen Verhältnisse im Raum der Ptolemais-Senke und des westlichen Vermiongebirges in Griechisch-Mazedonien. PhD Diss, Freie Univ Berlin [in German]

Parsian S, Amani M, Moghimi A, Ghorbanian A, Mahdavi S (2021) Flood hazard mapping using fuzzy logic, analytical hierarchy process, and multi-source geospatial datasets. Remote Sens 13:4761. https://doi.org/10.3390/rs13234761

Pavloudakis F, Roumpos C, Karlopoulos E, Koukouzas N (2020) Sustainable rehabilitation of surface coal mining areas: the case of Greek lignite mines. Energies 13(15):3995. https://doi.org/10.3390/en13153995

Pu F, Ding C, Chao Z, Yu Y, Xu X (2019) Water-quality classification of inland lakes using Landsat8 images by convolutional neural networks. Remote Sens 11:1674. https://doi.org/10.3390/rs11141674

Rad AM, Kreitler J, Sadegh M (2021) Augmented normalized difference water index for improved surface water monitoring. Environ Model Softw 140:105030. https://doi.org/10.1016/j.envsoft.2021.105030

Roumpos CP, Paraskevis NI, Galetakis MJ, Michalakopoulos TN (2015) Mineable lignite reserves estimation in continuous surface mining. In: Niemann-Delius C (ed) Proc, 12th International Symp on Continuous Surface Mining. Springer International Publishing, Cham, pp 177–194

Roumpos C, Sideri D, Pavloudakis F, Kolovos N, Michalakopoulos T, Galetakis M, Vafidis A (2018) Possibilities for improving work efficiency of continuous surface mining systems operating in rocks with excessive digging resistance. Gór Odkryw r 59:31–41

Rouse JW, Haas RH, Schell JA, Deering DW, Harlan JC (1974) Monitoring the Vernal Advancement and Retrogradation (Green Wave Effect) of Natural Vegetation. NASA Goddard Space Flight Centre, Greenbelt, Maryland, USA

Saha A, Patil M, Goyal VC, Rathore DS (2018) Assessment and impact of soil moisture index in agricultural drought estimation using remote sensing and GIS techniques. In: ECWS-3. MDPI, p 2

Sandholt I, Rasmussen K, Andersen J (2002) A simple interpretation of the surface temperature/vegetation index space for assessment of surface moisture status. Remote Sens Environ 79:213–224. https://doi.org/10.1016/S0034-4257(01)00274-7

Sohrabi MM, Ryu JH, Abatzoglou J, Tracy J (2015) Development of soil moisture drought index to characterize droughts. J Hydrol Eng 20:04015025. https://doi.org/10.1061/(ASCE)HE.1943-5584.0001213

Sonter LJ, Moran CJ, Barrett DJ, Soares-Filho BS (2014) Processes of land use change in mining regions. J Clean Prod 84:494–501. https://doi.org/10.1016/j.jclepro.2014.03.084

Stathopoulos N (2019) Research methods for geo-environmental hazards and water resources, in the hydrological basin of Sperchios river, utilizing geographic information systems and remote sensing. PhD Diss, Natl Tech Univ Athens, Sch Min Metall Eng [in Greek]

Tang Q, Qi Y, Wang Z, Pan Y (2020) Editorial for the special issue "remote sensing of the terrestrial hydrologic cycle." Remote Sens 12:1035. https://doi.org/10.3390/rs12061035

Vasileiou E, Papazotos P, Dimitrakopoulos D, Perraki M (2019) Expounding the origin of chromium in groundwater of the Sarigkiol basin, western Macedonia, Greece: a cohesive statistical approach and hydrochemical study. Environ Monit Assess 191:509. https://doi.org/10.1007/s10661-019-7655-1

Voudouris K, Mavrommatis Th, Antonakos A (2007) Hydrologic balance estimation using GIS in Korinthia prefecture, Greece. Adv Sci Res 1:1–8. https://doi.org/10.5194/asr-1-1-2007

Wanders N, Bierkens MFP, de Jong SM, de Roo A, Karssenberg D (2014) The benefits of using remotely sensed soil moisture in parameter identification of large-scale hydrological models. Water Resour Res 50:6874–6891. https://doi.org/10.1002/2013WR014639

Xu H (2006) Modification of normalised difference water index (NDWI) to enhance open water features in remotely sensed imagery. Int J Remote Sens 27:3025–3033. https://doi.org/10.1080/01431160600589179

Xu X, Li J, Tolson BA (2014) Progress in integrating remote sensing data and hydrologic modeling. Prog Phys Geogr Earth Environ 38:464–498. https://doi.org/10.1177/0309133314536583

Yan Y, Wang G, Nanding N, Chen W (2022) Hydrological evaluation of satellite-based precipitation products in Hunan Province. Remote Sens 14:3127. https://doi.org/10.3390/rs14133127

Yu Yangyang, Li Jiangfeng, Zhang Juan (2010) Effects of topography on land use pattern in karst areas. Proc, 2nd Conf on Environmental Science and Information Application Technology, IEEE, pp 760–763

Zhang Y, Zou J, Dang S, Osborne B, Ren Y, Ju X (2021) Topography modifies the effect of land-use change on soil respiration: a meta-analysis. Ecosphere. https://doi.org/10.1002/ecs2.3845

Zhao Y, Cao J, Zhang X, Zhang M (2022) Analyzing the characteristics of land use distribution in typical village transects at Chinese Loess Plateau based on topographical factors. Open Geosci 14:429–442. https://doi.org/10.1515/geo-2022-0370